Molecular dynamics simulation of nucleation in the binary mixture n-nonane/methane

Stephan Braun, Vitaly Kalikmanov, and Thomas Kraska

Citation: The Journal of Chemical Physics **140**, 124305 (2014); doi: 10.1063/1.4868963
View online: http://dx.doi.org/10.1063/1.4868963
View Table of Contents: http://scitation.aip.org/content/aip/journal/jcp/140/12?ver=pdfcov
Published by the AIP Publishing

Molecular dynamics simulation of nucleation in the binary mixture n-nonane/methane

Stephan Braun,[1] Vitaly Kalikmanov,[2] and Thomas Kraska[1,a)]
[1]*Institute for Physical Chemistry, University of Cologne, Luxemburger Str. 116, 50939 Köln, Germany*
[2]*Twister BV, Einsteinlaan 20, 2289 CC, Rijswijk, The Netherlands and Department of Geosciences, Delft University of Technology, Stevinweg 1, 2628 CN, Delft, The Netherlands*

(Received 28 October 2013; accepted 7 March 2014; published online 24 March 2014)

Vapor-liquid nucleation in the binary system n-nonane/methane is investigated by molecular dynamics simulation. The supersaturation is achieved by cooling down the system during the expansion in order to closely mimic the real process. Binary clusters formed by nucleation are frequently inhomogeneous objects in which components are not well mixed. By studying high-pressure nucleation and cluster growth in the n-nonane/methane mixture, we demonstrate the role of structuring effects in these processes. At typical simulation conditions—pressure 60 bar, temperature 240 K, and nucleation rate $\sim 10^{26}$ $cm^{-3}s^{-1}$—the mole fraction of methane in the critical cluster reaches 80 percent, which is much higher than its equilibrium value in the bulk liquid at the same pressure and temperature. These observations are supported by the recently formulated coarse-grained theory for binary nucleation as well as by the experimental observations. © *2014 AIP Publishing LLC*. [http://dx.doi.org/10.1063/1.4868963]

I. INTRODUCTION

Phase transitions take place via a complex kinetic process starting with nucleation in a supersaturated system and followed by the growth of the new phase via surface growth, agglomeration or coagulation, and ripening. In case of condensation, the system can be supersaturated by a fast expansion leading to cooling down. Experimentally, the pressure drop can be realized by a variety of methods: e.g., in an expansion cloud chamber[1] or in a supersonic nozzle.[2,3] The nucleation process is usually analyzed by optical detection of droplets using scattering techniques. However, it is rather difficult to detect and investigate the *critical clusters*, because their size ranges from a few atoms or molecules to about 100 at typical values of supersaturation. The critical cluster size is an important property: once a cluster has passed this size it is likely to continue growing to a stable bulk phase.[4] Therefore, the knowledge of the properties and the structure of the critical cluster is very important for a better understanding of nucleation processes[5] and further development of nucleation theories. There are various effects of the cluster structure which can influence the modeling of the nucleation process. One of such effects is a preferred orientation of molecules in the interface of a small cluster, which can affect the surface tension: for example, methanol molecules exhibit a preferred orientation of the CH_3 group towards the surface.[6] In case of a binary critical nucleus spatial distribution of species inside the cluster, found e.g., in water/butanol systems,[7] modifies the cluster properties compared to the two-phase bulk system. For the system n-nonane/methane, it has already been shown[8,9] that the composition and the structure of the clusters differ significantly from the bulk phase behavior. In this case, enrichment of methane molecules at the interface region has been found. Furthermore, the mole fraction of methane in the critical cluster is much higher than the fraction of methane in the equilibrium bulk liquid at the same pressure and temperature. Experimental data on the critical cluster properties are rare and often require much experimental effort.

Early approaches in binary nucleation theory[10,11] are extensions of the single-component classical nucleation theory (CNT)[12,13] and do not account for inhomogeneous cluster structures (adsorption effects). Later developments distinguish between the core and the surface of a cluster[14–16] by introducing a Gibbs dividing surface. Beyond that a transient state of the critical cluster, having a transient structure, was discussed.[17] A thorough treatment of adsorption effects combined with statistical-mechanical considerations applied to small clusters has been recently proposed in Ref. 18.

Theoretical work, such as molecular dynamics (MD) simulation, can contribute to the understanding of the nucleation process including the analysis of the critical cluster properties and the growth of these clusters to stable droplets. There are various methods of simulating the nucleation process. Besides Monte Carlo approaches for the determination of the activation barrier of the nucleation process,[19] MD simulations can be employed to study the dynamics of the nucleation process. It includes transient stages, which influence the growth of small entities of the new phase. In case of condensation, these are small liquid-like clusters growing to liquid droplets. Transient states can be the formation of a certain size-dependent structure which vanishes in the course of further growth.[17] These may be atomic ordering,[20] the above mentioned molecular ordering,[6] or demixing.[7] Such structures may not exist in the macroscopic phase and hence vanish during further growth. In recent years, several approaches to simulate the nucleation dynamics have been proposed. In

a)E-mail: t.kraska@uni-koeln.de

direct simulation of nucleation, an equilibrated stable system is transferred into a supersaturated state, for example, by instantaneously decreasing the temperature. Then, the change of the system on its way back to a new equilibrium state is observed. If the supersaturation of a vapor phase is high enough, eventually the system starts to form small clusters by fluctuations. Once the activation barrier for nucleation, being the minimum work of critical cluster formation, is overcome, the cluster on average grows continuously to a stable droplet.

Technically there are various ways to generate supersaturation in MD simulations. One can induce a temperature jump and then fix the temperature at a low value by a numerical thermostat. There are different ways for the implementation of such a thermostat. In case of weakly interacting systems, such as argon, a directly applied homogeneous thermostat may be reasonable. The simplest methods are the isokinetic direct velocity scaling or weak coupling by a Berendsen thermostat.[21] Other methods are the Nose-Hoover thermostat[22–24] affecting the forces and the stochastic Andersen thermostat.[25] In case of *strongly interacting* systems, these approaches are less appropriate.[20,26] The latent heat, set free during nucleation and growth, is very large leading to a strong temperature rise of the clusters which have just been formed. If the complete system, consisting of hot clusters and cold vapor, is cooled down homogeneously, the vapor phase atoms are artificially cooled down below the target temperature. In such systems, it is necessary to use a carrier gas thermostat.[20,27,28] The carrier gas itself is coupled to a thermostat, as described above, but the nucleating substance exchanges energy only by collisions with the carrier gas. This approach not only avoids the problems mentioned above, it is also closer to the experimental process, where usually a carrier gas is present.

In our work, cooling is caused by the expansion of the system.[29] Hence, one does not need to apply a thermostat either to the nucleating substance or to a carrier gas. In this context, we must distinguish between (i) systems with one nucleating substance and a passive carrier gas and (ii) binary nucleating systems. A system with a passive carrier gas actually exhibits a single-component nucleation: the carrier gas does not interfere with the nucleation process beyond its function as a heat transfer medium (removing the latent heat). In the case of (ii), both substances take part in the cluster formation. Besides cooling down, supersaturation in expanding binary systems can be influenced by the change in solubility. This is, for example, the case in the rapid expansion of a supercritical solution (RESS) process[30] where the rapid decrease of the solubility during the expansion is the main effect.

In the present work, we investigate the gas-liquid nucleation in the binary mixture of n-nonane and methane. Since the vapor mole fraction of methane is very high, the major cooling effect is related to the methane expansion. A pressure drop pushes the system into the binary two-phase equilibrium region, eventually leading to the phase separation. Both species take part in the cluster formation at the given external conditions; hence, we actually deal here with the process of binary nucleation.

For the determination of the nucleation rate based on molecular dynamics simulation, we employ the so-called *threshold method* of Yasuoka and Matsumoto.[28] It requires a sufficiently large simulation system in order to detect a certain amount of clusters formed by nucleation. In other words, the method represents an analysis of cluster statistics in the system. The amount of clusters with the size larger than a given threshold value is counted and plotted versus the simulation time. This is done for various threshold values for better statistics. These plots exhibit a linearly ascending domain which should be parallel for all threshold values. The slope of this linear domain is proportional to the nucleation rate. The critical cluster size can be calculated afterwards using the nucleation theorem[31] as it is done in the analysis of experimental nucleation isotherms. In addition, the cluster size statistics, especially the size fluctuation, can be related to the critical cluster size.[32] The threshold method is a quasi-stationary technique in the sense that within a certain time the system behaves close to the stationary state with a constant supersaturation and quasi-stationary nucleation. This falls into the linearly ascending domain of the Yasuoka-Matsumoto plot which is short enough to avoid the possible influence of cluster coalescence (see Chap. 8 of Ref. 4) (the latter appears later in the stagnating and descending domain of the Yasuoka-Matsumoto plot). In order to have a stationary system for a long period of time, one has to keep that state alive by interfering with the simulation system. Such an approach has been proposed by Horsch and Vrabec[33] who combined the grand canonical ensemble with the so-called *McDonald demon*[34] being a Maxwell demon for clusters. This demon cuts the cluster size distribution at a given size by removing clusters having reached that size. These clusters should be big enough to guarantee further growth to the stable droplets. The grand canonical treatment of the vapor phase replaces successively the atoms, which have been removed as a cluster from the system, by keeping the chemical potential constant. By doing so it is possible to maintain the state of the system for an arbitrarily long time at the expense of interfering the dynamics of the system. In this approach as well as in the quasi-stationary linear domain of the Yasuoka-Matsumoto plot cluster coalescence is unlikely.

Although the type of interactions in the two components of the system under study—n-nonane and methane—is quite similar, the system is asymmetric due to the difference in molecular sizes (or rather chain length) of the two species. This makes them immiscible over a wide range of pressures and compositions. From the point of view of applications, the system n-nonane/methane can serve as a simplified model for natural gas, containing predominantly methane and a small amount of heavy hydrocarbons. The experimental data of the system of interest corresponds to the vapor mole fraction of the heavy component—n-nonane—of the order of 10^{-4} [35,42,43] which is typical for the operating conditions of modern supersonic gas-liquid separators, manufactured by Twister BV, aiming at removal of heavy hydrocarbons and water from the natural gas.[36]

Looijmans *et al.*[37] included the real gas effects in the study of nucleation in the system n-nonane/methane by means of the Binary Classical Nucleation Theory (BCNT) (see, e.g., Chap. 11 of Ref. 4). Including the real gas effects is necessary because the condensation process takes place at high

pressures and high vapor-phase densities which are beyond the applicability of the ideal gas law. It was found that the mole fraction of methane in the critical cluster increases with the pressure but is always lower than in the equilibrium bulk liquid at the same pressure and temperature. Furthermore, they found that the increasing amount of methane decreases the surface tension and, hence, the nucleation rate increases at high pressures. Experimental data for the nucleation rates in the pressure ranging from 10 to 40 bar and temperature between 230 and 250 K have been reported by Luijten *et al.*[8] They found that the amount of methane in the critical cluster is *much larger* than in the corresponding equilibrium bulk phase, which is in contradiction with the results of Ref. 37. The authors attribute this disagreement to a possible cluster structure consisting of a cluster core with a lower methane concentration and a surface layer containing predominantly methane molecules. This is in agreement with recent work on the transient structure of the binary clusters in this system.[9] Luijten *et al.*[8] also found that no binary nucleation theory was able to model the experimental data and attribute that to the enhanced methane concentration in the critical cluster as suggested by the experiments. Later measurements of this system with an improved experimental technique[38] confirmed the earlier results. Using the thermodynamic considerations, Kalikmanov and Labetski[39] showed that at sufficiently high pressures, above the so called *compensation pressure*, the net effect of the unlike (in our case: n-nonane-methane) interactions in the mixture becomes so strong that it leads to the negative partial molecular volume of n-nonane in the vapor phase giving rise to an active entrainment of methane molecules into the cluster.

II. METHOD

For MD simulations of this work, the software package *Moscito* is used,[40] which we have further developed for the investigation of nucleation and growth and optimized to treat large system sizes. The quantitative molecular modeling of thermophysical properties by molecular simulation requires accurate force fields. In this work, we employ a potential model developed by Martin *et al.*,[41] the so called TraPPE-UA-model. This is a Lennard-Jones based potential model where every alkyl-segment is treated as a separate interaction site. The TraPPE-UA force field (UA = united atom) utilizes pseudo-atoms located at carbon centers of the different alkyl groups (CH_4, CH_3, CH_2). The Lennard-Jones parameters for these groups used in the TraPPE Force Field are presented in Table I. For interactions between different Lennard-Jones sites, the standard Lorentz-Berthelot combining rules are applied. The force field parameters for a certain interaction are transferable between different molecules.

TABLE I. Lennard-Jones parameters for the TraPPE Force Field for alkanes.

Pseudoatom	ε/k_B [K]	σ [Å]
CH_4	148	3.73
CH_3	98	3.75
CH_2	46	3.95

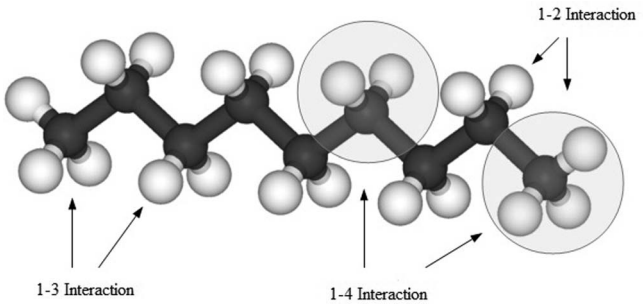

FIG. 1. Schematic sketch of the TraPPE interaction model for n-nonane.

The total potential energy is divided into a bonded and a non-bonded part. The *non-bonded contributions*, being the van der Waals interactions, are used only for the interactions of pseudo-atoms belonging to different molecules or belonging to the same molecule but not accounted for by any of the intramolecular bonded potentials. The intramolecular *bonded interaction* include three contributions[41] (see Fig. 1): (i) a fixed bond lengths of 0.154 nm for neighboring pseudo-atoms (1-2 interactions), (ii) harmonic angle bending potentials for pseudo-atoms separated by two bonds (1-3 interactions) with a force constant $k_\theta/k_B = 62500$ K rad^{-2} and an equilibrium angle $\theta_0 = 114^\circ$,

$$u_{\text{bend}} = k_\theta(\theta - \theta_0)^2/2,$$

(here k_B is the Boltzmann constant) and (iii) dihedral torsion potentials for pseudo-atoms separated by three bonds (1-4 interactions)[41],

$$u_{\text{tors}} = c_1[1 + \cos\phi] + c_2[1 - \cos(2\phi)] + c_3[1 + \cos(3\phi)]$$

with $c_1/k_B = 355.03$ K, $c2/k_B = -68.19$ K, and $c_3/k_B = 791.32$ K. For all simulations, we used a cutoff value of 1.4 nm. Hence, the non-bonded intramolecular interactions start with the 1-5 interaction and include all higher ones. This potential model has been chosen because its parameters have been fitted to the phase equilibrium data. Having correct phase equilibrium data is important for the calculation of the supersaturation of the system.

As it was noted, typical experimental values of the n-nonane mole fraction in the vapor at given conditions are very low being in the order of 10^{-4}. This requires a large amount of methane molecules in the simulation box. In order to keep the simulation feasible, we have used a one-site Lennard-Jones model for methane which is a quite good approximation at given conditions. The simulation systems consist of roughly 95 000 methane molecules with 125 to 343 n-nonane molecules leading to y_{C9} ranging between $1.3 \cdot 10^{-3}$ and $3.6 \cdot 10^{-3}$, which are still approximately 10 times higher than in experiment. The values of y_{C9} used in the simulations are presented in Table II. Variation of y_{C9} occurs as a result of our simulation procedure: the mixture is generated from pure methane by inserting n-nonane and deleting the methane molecules that overlap with the n-nonane molecules. The initial box size before the expansion ranges from 18 to 23 nm^3.

TABLE II. Nucleation rates obtained in the simulations. The physical properties are explained in the text.

Data point	y_{C9}	T_{start} [K]	ρ_{start} [mol/dm^3] of methane	T_{nuc} [K]	p_{nuc} [bar]	ρ_{nuc} [mol/dm^3] of methane	$\log_{10}(S_{C9})$	J [10^{26} cm^{-3}s^{-1}]
A	0.0036	320	13.28	274	48	2.47	1.36	2.02
B	0.0036	320	18.14	250	43	2.45	2.07	2.63
C	0.0036	320	25.87	240	55	3.66	2.13	8.51
D	0.0036	300	18.14	232	43	2.83	2.64	2.46
E	0.0036	300	25.87	220	46	3.66	2.93	10.06
F	0.0023	300	13.28	249	40	2.34	1.94	0.92
G	0.0023	300	18.14	234	51	3.50	2.18	2.33
H	0.0023	320	18.14	245	31	1.79	2.19	1.91
I	0.0023	300	25.87	216	44	3.45	2.92	3.55
J	0.0023	320	25.87	224	29	1.90	3.03	1.54
K	0.0013	300	18.14	220	32	2.12	2.89	1.12
L	0.0013	300	25.87	202	29	2.30	3.76	1.66

The time step for solving the equations of motion is 1 fs in all simulations.

A. Expansion simulation

For the simulation of the expanding solution, we employ a recently developed method for the simulation of the rapid expansion of a super critical solution (RESS) process.[30] The expansion is simulated via a stepwise enlargement of the simulation box with short equilibration runs in between. After the NVT equilibration simulation, followed by a short NVE equilibration run, the box is expanded by 0.1 nm in all three dimensions. At each expansion step a short NVE simulation over 3.5 ps is performed. After this run, the box is expanded again followed by another NVE run, and so on. Depending on the enlargement step and the time period for the NVE run at each expansion step, the velocity of the expansion can be varied. In a detailed study,[30] it was found that around 100 expansion steps are sufficient.

B. Cluster detection

In order to locate clusters in the simulation system, analyze cluster statistics, and calculate the nucleation rate, an algorithm for the detection of a cluster has to be implemented. Several cluster definitions suitable for the given system are available in the literature (see Chap. 8 of Ref. 4). Here we use the distance criterion of Stillinger[44] extended by the *life-time criterion*.[30] Within the Stillinger definition, two atoms belong to the same cluster if their separation is smaller than a given distance r_{St}. Its value is typically in the order of 1.5 times of the atomic diameter. The factor 1.5 is somewhat arbitrary, but usually its variation between 1.2 and 1.8 does not affect the results significantly. Within the Stillinger definition, two atoms passing by or colliding with high energy are also accounted as a cluster. This leads to some fluctuations in the cluster size, which usually do not affect the result. We here extend the cluster definition by a life-time criterion: two atoms belong to the same cluster if they remain closer than r_{St} during a certain life-time τ_{LT}. One can estimate τ_{LT} from the atomic velocities using the kinetic gas theory.[30] This gives typically the value τ_{LT} in the range 1-2 ps. Here we use $\tau_{LT} = 2$ ps which we have found as a suitable value for the given system.

III. RESULTS AND DISCUSSION

A. Expansion of pure methane

Methane is the abundant component in natural gas while the n-nonane vapor mole fraction is very low: the ratio of n-nonane to methane molecules is in the order of 1:10^4. Therefore, it can be expected that the properties of the mixture in the vapor phase are dominated by methane. Furthermore, expansion simulations of pure methane are required to agree with the adiabatic path of the expansion process. Not all properties needed for the calculation of the adiabatic curve of the n-nonane/methane mixture are available, whereas there are accurate equations of state (EoS) for methane.[45] Therefore, the single-component system serves as a quantitative test for the expansion method: through its comparison with the expansion of the actual binary system one is able to distinguish the effects caused by interactions between the two species and internal degrees of freedom.

Calculations of pure methane require less computational power, since methane is treated as a united-atom Lennard-Jones site. This is a feasible way to analyze fundamental aspects of the expansion simulation method for the system under investigation. The method has so far been tested only for carbon dioxide[30] modeled by an electrostatic model—in contrast to Lennard-Jones methane used in the present study. Quantitative differences between these substances are expected, for example, in the extent of cooling due to the expansion. Therefore, we have performed different expansions with pure methane at different initial conditions. The methane density varied in a range from 6.25 to 25 mol/dm^3 and the temperature varied in a range from 220 to 260 K. The resulting initial pressures varied from 10 to 60 MPa. Furthermore, the time period for each NVE run at each expansion step varied from $\tau(\text{NVE}) = 1.5$ to 5 ps.

With respect to the time period of the NVE simulation at each expansion step, a limitation of the simulation method can be observed. If the expansion of the system is too fast, i.e., the time of the NVE simulation at each expansion step,

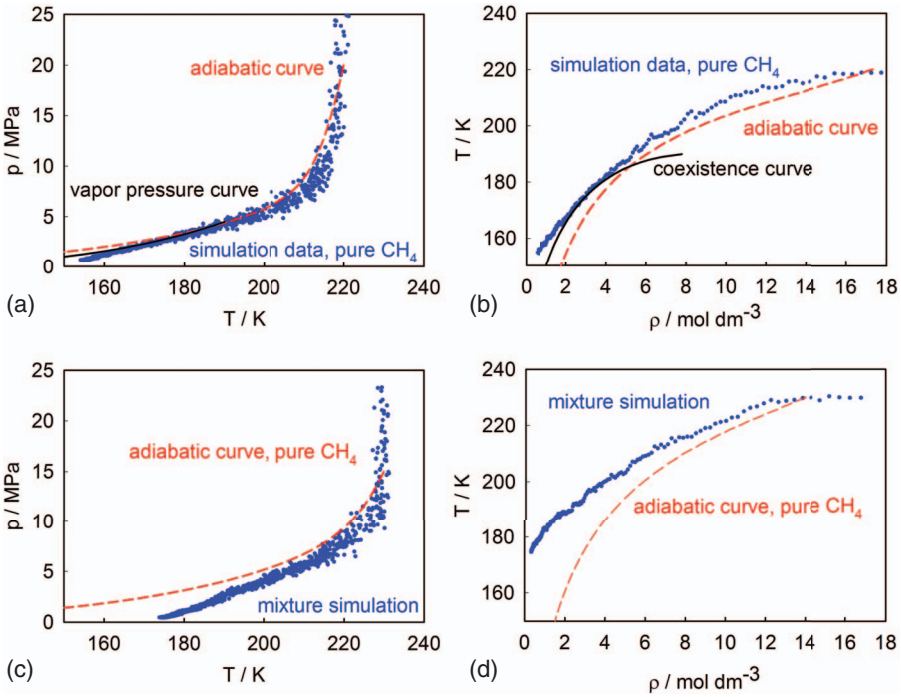

FIG. 2. Example for an expansion simulation (points) of pure methane (a) and (b) and binary mixture n-nonane/methane (c) and (d). The initial conditions of this example run are: $T = 230$ K, $\rho = 25.87$ mol/cm^3. Also shown are the adiabatic (isentropic) curve for pure methane calculated from the Setzmann-Wagner reference EoS[45] (dashed lines) and the coexistence curve for pure methane calculated with the same EoS (solid line in (a) and (b)).

τ(NVE), is too short, one can observe the leftover of a condensed phase in the form of a cluster in the middle of the box. This cluster did not originate through the "normal" growth mechanism, but is an artifact of the chosen value of τ(NVE) because the system just did not have enough time to equilibrate. Hence, small τ(NVE) yield inhomogeneous distribution of the methane molecules within the box. If the expansion is carried out with a larger τ(NVE), then at the same initial conditions (temperature, pressure, density) one observes a homogeneous expansion.

We have compared the expansion data from MD with the adiabatic (isentropic) expansion curve and the vapor pressure curve calculated with the reference equation of state of Setzmann and Wagner.[45] The aim of the comparison is to check whether the model is able to represent the expansion of the real system. This accounts for inaccuracies of the potential parameters as well as the different degrees of freedom of real methane and the united atom model resulting in different heat capacity ratios. The results are shown in Figs. 2(a) and 2(b). One can see a good agreement of the simulation results with the reference EoS in the pressure-temperature plot (Fig. 2(a)). There is, however, a parallel shift of the expansion curve in the temperature-density diagram (Fig. 2(b)). This shift is related to a relatively strong change in the state conditions in the first expansion step. Still the curves are close and parallel showing that the simulation expansion path is meaningful. One can also see that the expansion path does not cross the coexistence curve, i.e., methane remains in the one-phase region.

B. Expansion of the binary mixture

In the expansion simulations of the mixtures, one can observe similar effects as for the expansion of pure methane. Again, a too short NVE simulation with of τ(NVE) = 2.5 ps between each expansion step results in a cluster leftover induced by the simulation method. If one increases the equilibration time to 3.5 ps, realistic cluster growth can be observed. One gets a homogeneous phase with several nucleation events leading to many small clusters. Due to the lack of an accurate reference equation of state for the binary system n-nonane/methane, we compared the results of MD simulation with the adiabatic expansion of the pure methane shown in Figs. 2(a) and 2(b). As an example, the results for a binary system are shown in Figs. 2(c) and 2(d). The deviation of the MD simulations of the mixture from those of the pure substance is caused by the added n-nonane molecules. In the temperature-density plot, the curves are shifted being not parallel as for pure methane.

It should be noted that the chosen method of generating the supersaturation by expansion does not allow imposing the desired values of temperature T and pressure p at the onset of nucleation. It is only possible to choose the *initial conditions* at high pressure. Therefore, the values for T and p result from the simulation and are not predefined.

To be sure that cluster formation takes place only during the expansion simulation, we analyzed the cluster statistics in the initial system and found that the cluster size in the initial system was typically two (n-nonane dimers) with some fluctuations. We carried out simulation runs of about 0.5 ns before each expansion simulation and did not observe the formation of a stable cluster of n-nonane in the initial solution.

C. Calculation of the supersaturation

For the calculation of the supersaturation, the equilibrium vapor mole fractions are required. The available experimental

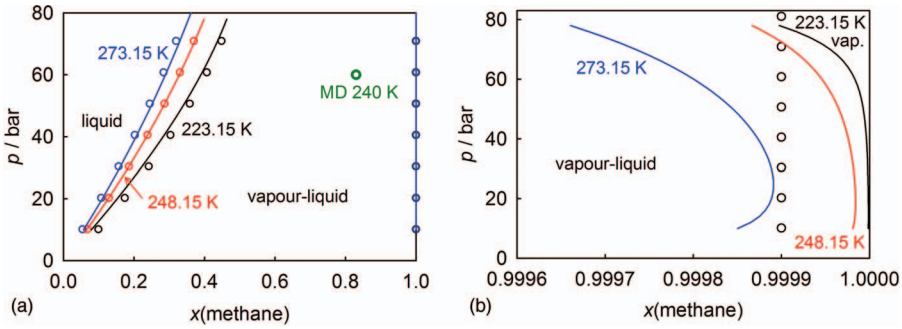

FIG. 3. (a) Bulk phase diagram of the n-nonane/methane system for three different temperatures.[35] The green point marks the mole fraction of the critical cluster during nucleation simulation (MD: 240 K). The arrow indicates the equilibrium phase mole fraction of methane in the bulk liquid corresponding to the nucleation conditions (240 K, 60 bar) studied in the MD simulations. The curves are correlations with the PC-SAFT equation of state. (b) Enlargement of the methane-rich part of the phase diagram.

data for the methane vapor mole fraction are approximately $y_{C1,eq} \approx 0.9999$ independent of pressure and temperature[35] (see Fig. 3(b)) which makes it difficult to determine the n-nonane equilibrium vapor fraction $y_{C9,eq} = 1 - y_{C1,eq}$ at the given p and T. That is why for equilibrium calculations, we use the PC-SAFT equation of state,[46,47] which is particularly suitable for modeling the chain molecules like n-alkanes. Even though PC-SAFT has some deviation from the experimental data in the vapor branch of the phase diagram, it reproduces the trend properly (see Fig. 1 from Ref. 35) and is more suitable for the calculation of the supersaturation than the low-resolution experimental data. The correlation of the experimental data on the liquid side, in the pressure region of interest, is quite accurate as one can see from Fig. 3(a). Deviations appear at pressures above 100 bar and in the critical region, which is typical for classical (mean-field) equations of state. Since PC-SAFT, as well as TraPPE, properly describes the experimental data, we can use it for the calculation of the supersaturation in the simulation system. The parameters of the pure substances (n-nonane and methane) are taken from the original papers on PC-SAFT[46,47] while we fit the binary interaction parameter $T_{12}{}^*$. All parameters are listed in Table III. The supersaturation S_{C9} of n-nonane is given by (Chap. 13 of Ref. 4)

$$S_{C9} = \frac{y_{C9}}{y_{C9,eq}(p, T)}, \tag{1}$$

where $y_{C9,eq}(p, T)$ is calculated by means of the PC-SAFT EoS. The values for p and T are averaged over the period of nucleation, i.e., over the linear domain in the Yasuoka-Matsumoto plot. For example, in Fig. 4, p and T are averaged over the period from 0.4 to 0.65 ns corresponding to the linear domains for clusters larger than 4, 6, 8 n-nonane molecules, etc. In this specific case, the values at the beginning of the linear domain at 0.4 ns are $T = 228$ K and $p = 60$ bar and the averaged values are $\bar{T} = 220$ K and $\bar{p} = 46$ bar. This gives a variation in the supersaturation of 0.30 on the logarithmic scale for this specific configuration, where the average variation/uncertainty in the supersaturation over all simulation runs is 0.16. This difference may be regarded as the variation of the supersaturation during the nucleation period rather than an error of the supersaturation.

TABLE III. Parameters for the PC-SAFT equation of state used here.[46,47] T^* is the attraction parameter and b the covolume parameter.

	$T_{ij}{}^*$/K	b_{ij}/cm^{3}mol^{-1}
methane	150.03	16.0224
n-nonane	244.51	17.9213
Cross interaction	188.64	16.9719

D. Nucleation

To analyze nucleation rates J, we apply the method of Yasuoka and Matsumoto[28] plotting the number of clusters containing a number of n-nonane molecules larger than a certain threshold value n_{thres} as a function of time. Since the composition of the cluster is approximately constant during the nucleation period,[9] one can use the number of n-nonane molecules in the largest cluster for the Matsumoto-Yasuoka plot also for the estimation of the binary nucleation rate. In our case, we analyzed clusters larger than 2, 4, 6, 8, 10, and 12 n-nonane molecules. The slopes in the linear domain (see Fig. 4) yield the nucleation rate (see, Chap. 8 of Ref. 4)

$$J = \frac{1}{V_{box}} \frac{\partial}{\partial t} N_{\sum}(n_{thres}, t). \tag{2}$$

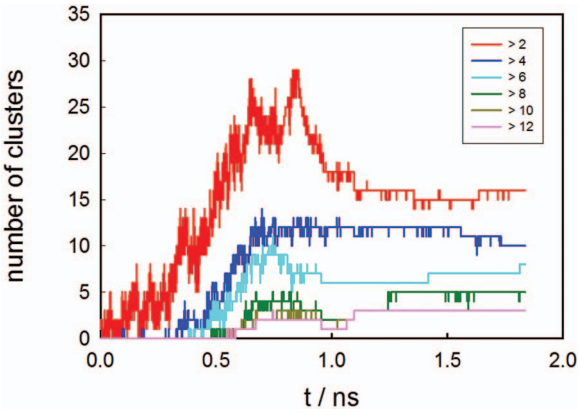

FIG. 4. Yasuoka plots for an expansion of a system consisting of 94450 methane + 343 n-nonane molecules, x(n-nonane) = 0.0036, with the initial conditions $T = 300$ K and $\rho(CH_4) = 25.87$ mol/dm^3.

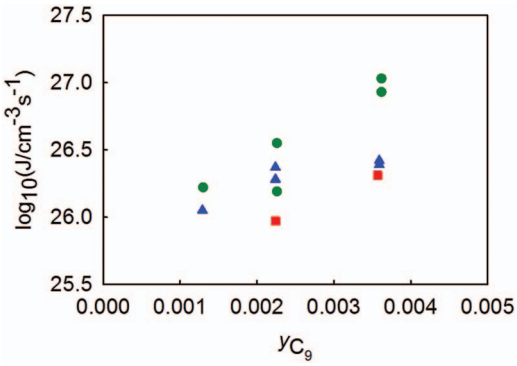

FIG. 5. Nucleation rates for different mole fractions and different initial methane densities (circles: 25.87, triangles: 18.14, squares: 13.28 mol/dm^3).

Here $N_{\sum}(n_{thres}, t)$ is the number of all clusters larger than n_{thres} at time t and V_{box} is the volume of the simulation box. The slopes of the curves for various threshold values in the linear domain are approximately equal (except for a little variation due to a regular uncertainty of the method). The nucleation rates for different mole fractions, different densities ρ_{start}, and temperatures T_{start} at the beginning of the expansion are listed in Table II.

Figures 5 and 6 show the nucleation rates J as a function of y_{C9} and S_{C9}, respectively. To get a closer look at the trends in J, we compare the results for different values of the initial density of methane in the system (indicated by different symbols in Fig. 6(a)). One can observe that the initial density of methane has small influence on J. Actually, the variation of a nucleation rate about one order of magnitude is the typical fluctuation for nucleation simulation results. Figure 6(b) shows the results for J obtained for different vapor mole fractions of n-nonane, y_{C9}. One can recognize a trend towards higher nucleation rates for higher y_{C9} at fixed S_{C9}. Due to the simulation setup, nucleation starts at different conditions; for each data point, the temperature (in K) and the pressure (in bar) are indicated in Table II. Due to the large amount of state variables characterizing a simulation run, it is difficult to plot these data more systematically.

It has already been shown that the binary clusters are structured.[9] In addition, the composition of the critical cluster, i.e., the mole fractions of components, can differ significantly from that of the equilibrium liquid phase. These two facts are expected to affect the nucleation process and hence the nucleation rate. We compare our simulation results with predictions of the recently formulated coarse-grained theory of binary nucleation (CGNT).[18] The latter takes into account inhomogeneous distribution of molecules within an arbitrary (n_a,n_b)-cluster (a = n-nonane, b = methane) by discriminating between the *bulk* and *excess* quantities of each species in the cluster using the general formalism of the Gibbs dividing surface:

$$n_i = n_i^l + n_i^{\text{exc}} \quad i = \text{a,b}. \tag{3}$$

The excess numbers n_i^{exc} are found by choosing the equimolar surface for the mixture, known as the K-surface,[48] defined as

$$\sum n_i^{\text{exc}} v_i^l = 0,$$

where v_i^l is the partial molecular volume in the liquid phase (for calculation of v_i^l, see Appendix D of Ref. 4). Its combination with the Gibbs adsorption equation yields the excess numbers n_a^{exc} and n_b^{exc}. The Gibbs free energy of an arbitrary binary cluster formation $g = \Delta G/k_B T$ is a function of the *total* numbers n_a, n_b as well as the bulk composition of the cluster $x_b^l = n_b^l/(n_a^l + n_b^l)$,

$$g(n_a, n_b; x_b^l) = -\sum_{i=\text{a,b}} n_i \ln S_i + g_{eq}, \tag{4}$$

$$g_{eq} = -\sum_{i=a,b} n_i \quad \ln\left[\frac{y_{i,\text{eq}}\, p}{y_i^{coex}\left(x_b^l, T\right) p_i^{coex}\left(x_b^l, T\right)}\right] + \theta_{micro,a}\left[\overline{n_a^s} - 1\right]. \tag{5}$$

The first term in Eq. (4) is the non-equilibrium part of g containing the supersaturations S_i of the components. The equilibrium part g_{eq} consists of the bulk and surface contributions. The bulk contribution (first term in Eq. (5)) results from the difference in the bulk composition between the given cluster and the equilibrium bulk liquid at T and p. Here $p^{\text{coex}}(x_b^1, T)$ is the total pressure above the binary bulk liquid solution with composition x_b^l and $y_i^{coex}(x_b^l, T)$ is the corresponding vapor phase fraction of component i. Note that this term can be both positive and negative.

The surface contribution (second term in Eq. (5)) is obtained using coarse-graining of the configuration integral of

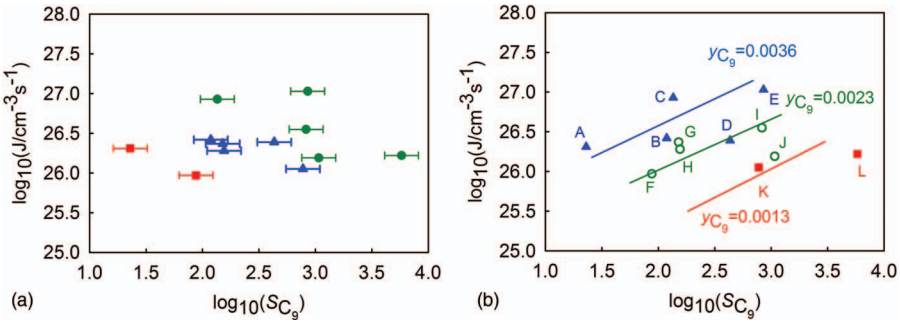

FIG. 6. Nucleation rates plotted versus the supersaturation in a double logarithmic plot. (a) The symbol styles indicate the different initial methane densities (circles: 25.87, triangles: 18.14, squares: 13.28 mol/dm^3). (b) Same data as in (a) but ordered by mole fractions. For each data point the conditions at the onset of nucleation are indicated by labels corresponding to Table II. The symbol styles indicates different initial mole fractions (circles: $y(C_9) = 0{,}0023$, triangles: $y(C_9) = 0.0036$, squares: $y(C_9) = 0.0013$). Error bars as in Fig. 6(a).

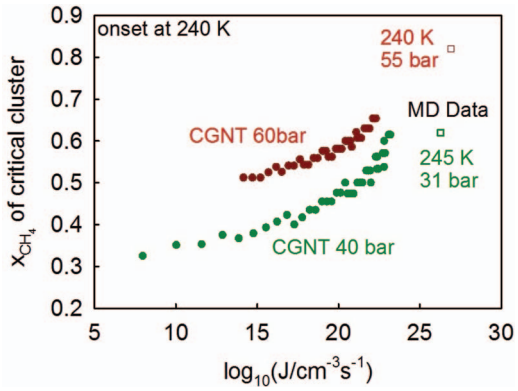

FIG. 7. Mole fraction of methane in the critical cluster as function of the nucleation rate. The circles are calculations with CGNT[18] and the squares are typical MD data points. For each MD-data point temperature and pressure for the onset of nucleation are indicated.

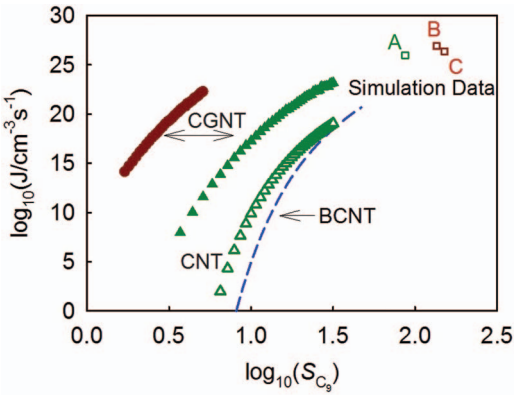

FIG. 8. Nucleation rate as function of the supersaturation of n-nonane. All theoretical calculations are performed for $T = 240$ K. Closed circles and closed triangles are calculations by means of CGNT[18] for $p = 60$ bar and 40 bar, respectively. Open triangles are calculations by means of effective CNT (see explanations in the text) for $p = 40$ bar. Blue dashed curve represents calculations by means of BCNT for $p = 40$ bar. The squares are typical MD data points. For each MD-data point temperature and pressure for the onset of nucleation are presented in Table IV.

the binary (n_a,n_b)-cluster. It is based on tracing out the degrees of freedom of the more volatile component (b, here: methane). As a result of coarse-graining, one is left with the configuration integral of the single-component cluster of pseudo-a molecules with the interaction energy implicitly depending on the mole fraction of substance b in the original binary cluster. The configuration integral of n_a-cluster is treated by means of the *mean field kinetic nucleation theory*:[49] $\theta_{\text{micro,a}}(x_b^{\text{l}})$ is the so-called "*reduced microscopic surface tension*" being the dimensionless (in the units of k_BT) mean free energy per surface molecule and $n_a^{\text{s}}(n_a, x_b^{\text{l}})$ is the number of surface molecules in the n_a-cluster.

The critical cluster of the binary system corresponds to the saddle point of g in the space of the total numbers of molecules of each species. The nucleation rate reads (for details see Chap. 13 of Ref. 4)

$$J = \nu_{\text{av}}\, A^*\, Z^*\, C\left(x_b^{\text{l}*}\right)\, e^{-g(n_a^*, n_b^*)}, \tag{6}$$

where the star refers to the critical cluster and ν_{av} is the average impingement rate per unit surface; A^* is the cluster surface area and Z^* is the Zeldovich factor. Furthermore,

$$C\left(x_b^{\text{l}*}\right) = \beta y_a^{\text{coex}}\left(x_b^{\text{l}*}\right)\, p^{\text{coex}}\left(x_b^{\text{l}*}\right) \text{ with } \beta = \frac{1}{k_B T}. \tag{7}$$

We performed CGNT calculations for the n-nonane/methane system using the Redlich-Kwong-Soave EoS.[50] Figure 7 shows the CGNT predictions for the total (bulk + excess) fraction of methane in the critical cluster as a function of the nucleation rate at the nucleation conditions $T = 240$ K, $p = 40$ and 60 bar. The theory suggests an increasing total methane fraction in the critical cluster with increasing nucleation rate.

Results obtained in MD simulations for approximately the same (p,T) points—(245 K, 31 bar) and (240 K, 55 bar)—are also indicated in Fig. 7. Due to the methodology of simulations, the nucleation rate is at the upper end but it fits into the trend of increasing the methane mole fraction in the critical cluster beyond its equilibrium value at corresponding values of p and T.

The total mole fraction of methane in the critical cluster at $p = 55$ bar, $T = 240$ K, obtained in the simulations, is about 0.8; it is indicated at the bulk phase diagram in Fig. 3(a) by the circle labeled "MD 240 K." The temperature at the onset of nucleation, 240 K, is close to the equilibrium isotherm 248.15 K (Figs. 3(a) and 3(b)) which at $p = 60$ bar gives a mole fraction of methane in the bulk liquid of about 0.3. It confirms the conjecture that the methane mole fraction in the critical cluster can be significantly higher than in the bulk phase.

Figure 8 shows the nucleation rates, predicted by the CGNT as a function of the supersaturation of n-nonane at $T = 240$ K and pressures of 40 and 60 bar. Also shown are predictions of the Binary Classical Nucleation theory (BCNT)[10,11] and an *effective single-component* CNT. Within the latter approach, the single-component properties in CNT are replaced by the corresponding properties of the binary mixture. For the sake of consistency, BCNT and CNT calculations are performed using the same Redlich-Kwong-Soave EoS as in CGNT. Also shown in Fig. 8 are exemplary MD-results corresponding to approximately the same (p,T) points. Due to the high supersaturation in MD simulations, the calculated nucleation rates are very high; nevertheless one can notice a good agreement with the CGNT by trend.

Predictions of BCNT and CNT differ significantly from the CGNT and the MD results. The major reason is that critical clusters, corresponding to the saddle point of the free energy, are sufficiently small objects implying that their surface energy should be described in terms of the *microscopic* surface tension, as in CGNT, rather than the *macroscopic* surface tension as in the phenomenological classical models. The model for the free energy, in turn, determines the location of the saddle point and hence the nucleation barrier;

TABLE IV. MD-data point temperature and pressure for the onset of nucleation.

Data point	T/K	p/bar
A	249	40
B	240	55
C	234	51

saddle points found in CGNT differ from the classical theory predictions. The lower surface energy of the critical cluster predicted by CGNT compared to CNT and BCNT shifts the nucleation rate towards higher values.

IV. CONCLUSIONS

The results presented here show that microscopic effects significantly influence the nucleation in a binary system. This appears to be the case especially if nucleation takes place under high pressure. Increasing pressure leads to an increasing amount of the more volatile substance in the forming clusters. On one hand, this reflects the trend of the bulk phase behavior that also exhibits an increasing mole fraction of the more volatile methane in the equilibrium liquid phase. In addition, there is a significant excess of the amount of methane in the cluster compared to the bulk phase. Enrichment of methane in the surface region of the cluster either by adsorption or by phase separation in a finite size system is observed. All these microscopic details affect the properties that govern nucleation and hence influence the nucleation rate.

Although CGNT is superior to the classical models due to the incorporation of microscopic properties, some deviations to the simulation results remain. MD simulation results indicate that the total molar fraction of methane in the critical cluster is higher than predicted by CGNT. Partly this can be explained by the difference in external conditions between simulations and theory: simulations were performed for very high supersaturation $S_{C9} \sim 200$–300 resulting in high nucleation rates $J \sim 10^{26}$–10^{28} $cm^{-3}s^{-1}$ compared to the range of reliable theoretical predictions $J < 10^{21}$–10^{22} $cm^{-3}s^{-1}$, corresponding to $S_{C9} < 50$–60. Going to higher theoretical supersaturation causes numerical instabilities in searching of the saddle point of the free energy. It is therefore desirable to perform simulations yielding lower nucleation rates, in the range of $J \sim 10^{21}$–10^{22} $cm^{-3}s^{-1}$, to be able to carry out direct comparison with the theory.

However, this explanation is not fully satisfactory. A weak point in CGNT, which may cause the discrepancy in the methane content of the cluster, is the calculation of the excess numbers of molecules n_i^{exc} for an arbitrary cluster with a bulk composition (n_a^1, n_b^1). This is done solving the linear set of equations consisting of the *K*-surface definition and the Gibbs adsorption equation (see Chap. 11 of Ref. 4 for the details). Both these equations involve the macroscopic properties, in first place the plane layer surface tension, which can become dubious when applied to small clusters. Moreover, a model for activity coefficients in the liquid is required. If n_i^{exc} derived using this procedure turns out not to be small compared to the bulk numbers, this approach can fall apart.[51]

ACKNOWLEDGMENTS

We gratefully acknowledge the support of this work by Twister B. V., The Netherlands.

[1] P. E. Wagner and R. Strey, J. Chem. Phys. **80**, 5266 (1984).
[2] Y. J. Kim, B. E. Wyslouzil, G. Wilemski, J. Wölk, and R. Strey, J. Phys. Chem. A **108**, 4365 (2004).
[3] W. Christen and K. Rademann, Phys. Scr. **80**, 048127 (2009).
[4] V. I. Kalikmanov, *Nucleation theory* (Springer, Dordrecht, 2013).
[5] R. Zhang, Science **328**, 1366 (2010).
[6] F. Römer, B. Fischer, and T. Kraska, Soft Mater. **10**, 130 (2012).
[7] B. E. Wyslouzil, G. Wilemski, R. Strey, C. H. Heath, and U. Dieregsweiler, Phys. Chem. Chem. Phys. **8**, 54 (2006).
[8] C. C. M. Luijten, P. Peeters, and M. E. H. van Dongen, J. Chem. Phys. **111**, 8535 (1999).
[9] S. Braun and T. Kraska, J. Chem. Phys. **136**, 214506 (2012).
[10] H. Reiss, J. Chem. Phys. **18**, 840 (1950).
[11] D. Stauffer, J. Aerosol Sci. **7**, 319 (1976).
[12] W. Volmer and A. Weber, Z. Phys. Chem. **119**, 277 (1926).
[13] R. Becker and W. Döring, Ann. Phys. **24**, 719 (1935).
[14] G. Wilemski, J. Chem. Phys. **80**, 1370 (1984).
[15] G. Wilemski, J. Phys. Chem. **91**, 2492 (1987).
[16] G. Wilemski, J. Chem. Phys. **88**, 5134 (1988).
[17] D. H. Rasmussen, J. Chem. Phys. **85**, 2272 (1986).
[18] V. I. Kalikmanov, Phys. Rev. E **81**, 050601(R) (2010).
[19] A. Lauri, J. Merikanto, E. Zapadinsky, and H. Vehkamäki, Atmos. Res. **82**, 489 (2006).
[20] N. Lümmen and T. Kraska, Nanotechnology **15**, 525 (2004).
[21] H. J. C. Berendsen, J. P. M. Postma, W. F. van Gunsteren, A. DiNola, and J. R. Haak, J. Chem. Phys. **81**, 3684 (1984).
[22] S. Nosé, Mol. Phys. **52**, 255 (1984).
[23] W. G. Hoover, Phys. Rev. A **31**, 1695 (1985).
[24] W. G. Hoover, Phys. Rev. A **34**, 2499 (1986).
[25] H. C. Andersen, J. Chem. Phys. **72**, 2384 (1980).
[26] P. Erhart and K. Albe, Appl. Surf. Sci. **226**, 12 (2004).
[27] J. Westergren, H. Grönbeck, S.-G. Kim, and D. Tománek, J. Chem. Phys. **107**, 3071 (1997).
[28] K. Yasuoka and M. Matsumoto, J. Chem. Phys. **109**, 8451 (1998).
[29] C. Kittel and H. Kroemer, *Thermal Physics* (W. H. Freeman, New York, 1980).
[30] F. Römer and T. Kraska, J. Phys. Chem. C **113**, 19028 (2009).
[31] D. Kashchiev, J. Chem. Phys. **76**, 5098 (1982).
[32] N. Lümmen and T. Kraska, Nanotechnology **16**, 2870 (2005).
[33] M. Horsch and J. Vrabec, J. Chem. Phys. **131**, 184104 (2009).
[34] J. E. McDonald, Am. J. Phys. **31**, 31 (1963).
[35] L. M. Shipman and J. P. Kohn, J. Chem. Eng. Data **11**, 176 (1966).
[36] V. Kalikmanov, M. Betting, J. Bruining, and D. Smeulders, *Society of Petrolem Engineers (SPE) Annual Technical Conference and Exhibition*, Anaheim, California, USA, 11–14 November 2007 (Paper No.: SPE 110736).
[37] K. N. H. Looijmans, C. C. M. Luijten, G. C. J. Hofmans, and M. E. H. van Dongen, J. Chem. Phys. **102**, 4531 (1995).
[38] P. Peeters, J. Hruby, and M. E. H. van Dongen, J. Phys. Chem. B **105**, 11763 (2001).
[39] V. I. Kalikmanov and D. G. Labetski, Phys. Rev. Lett. **98**, 085701 (2007).
[40] D. Paschek and A. Geiger, *MOSCITO 4* (Department of Physical Chemistry, University of Dortmund, 2002).
[41] M. G. Martin and J. I. Siepmann, J. Phys. Chem. B **102**, 2569 (1998).
[42] C. C. M. Luijten, Ph.D. thesis, Eindhoven University, 1999.
[43] D. G. Labetski, Ph.D. thesis, Eindhoven University, 2007.
[44] F. H. Stillinger, J. Chem. Phys. **38**, 1486 (1963).
[45] U. Setzmann and W. Wagner, J. Phys. Chem. Ref. Data **20**, 1061 (1991).
[46] J. Gross and G. Sadowski, Fluid Phase Equilib. **168**, 183 (2000).
[47] J. Gross and G. Sadowski, Ind. Eng. Chem. Res. **40**, 1244 (2001).
[48] A. Laaksonen, R. McGraw, and H. Vehkamaki, J. Chem. Phys. **111**, 2019 (1999).
[49] V. I. Kalikmanov, J. Chem. Phys. **124**, 124505 (2006).
[50] R. C. Reid, J. M. Prausnitz, and B. E. Poling, *The Properties of Gases and Liquids*, 4th ed. (McGraw-Hill, New York, 1987).
[51] H. Vehkamaki, *Classical Nucleation Theory in Multicomponent Systems* (Springer-Verlag, Berlin, 2006).